

## PAPER



Cite this: *Soft Matter*, 2019, 15, 8272

## Endocuticle sclerotisation increases the mechanical stability of cuticle

Lu-Yi Wang,<sup>id abc</sup> Mohsen Jafarpour,<sup>id d</sup> Chung-Ping Lin,<sup>id c</sup> Esther Appel,<sup>a</sup> Stanislav N. Gorb<sup>id a</sup> and Hamed Rajabi<sup>id \*a</sup>

The cuticle plays an important role in the evolutionary success of insects. Many studies on insect cuticles have reported a soft, resilin-rich endocuticle. However, a recent study indicated the presence of a sclerotised endocuticle in the weevil *Pachyrhynchus sarcitis kotoensis*, which contradicts former knowledge. To understand the degree of sclerotisation in the endocuticle of the weevil and its potential function, we first examined the endocuticle by microscopic and staining techniques. We next performed mechanical tests to measure the material properties of the endocuticle, and numerical simulations to predict the structural effect of the sclerotisation. Our results provide the first evidence of the existence of a sclerotised endocuticle and its remarkable function in improving the mechanical stability of the cuticle. This study highlights the finding of a high degree of sclerotisation in the stiff endocuticle of the weevil, especially the matrix surrounding the fibres. This novel case brings new understanding of cuticle properties and gives promising insights into biomaterial design.

Received 20th August 2019,  
Accepted 14th September 2019

DOI: 10.1039/c9sm01687b

rsc.li/soft-matter-journal

### 1. Introduction

Insects are one of the most successful taxa with more than one million described species.<sup>1–3</sup> They have colonized a wide variety of habitats since 400 million years ago.<sup>2</sup> One of the key innovations responsible for the impressive success of insects is their light-weight but robust exoskeleton.<sup>1</sup> The exoskeleton forms their body, protects them against mechanical damage, prevents pathogen intrusion and dehydration, contributes to the supplementary structures of sensory organs, and facilitates locomotion.<sup>2,4,5</sup> The importance of the insect exoskeleton becomes particularly clear when considering its role as a protective shield against predators.

The insect exoskeleton is made up of cuticle, a composite material, which is traditionally subdivided into three main layers, namely the epi-, exo-, and endocuticle (exterior to interior) based on their material composition and structure.<sup>6,7</sup> The two outermost layers (*i.e.* epi- and exocuticle) are known to be hard and dehydrated. The endocuticle, in contrast, is regarded as a soft layer enriched with resilin, a rubber-like protein.<sup>2,8–13</sup> While the epicuticle is cement-like and has no layered microstructure, the remaining two layers contain sublayers which are made of chitinous fibres.<sup>5</sup> The sublayers in the exocuticle are thin and dense. However, those in the endocuticle are thicker and composed of

large fibres (also called ‘macrofibrils’,<sup>6,14</sup> ‘microfibrils’,<sup>15</sup> or ‘macro-fibres’<sup>16</sup>) with pronounced protein matrix in between<sup>6,17</sup> (Fig. 1). Layers of fibres rotate in certain angles and are connected to each other *via* inter- and intra-ply cross-links.<sup>14,17</sup> This structure provides mechanical support to the insect exoskeleton.<sup>14,18,19</sup>

An example which well represents the function of the exoskeleton in defence is the cuticle of the weevil *Pachyrhynchus sarcitis kotoensis* (Coleoptera: Curculionidae). The exoskeleton of this species provides effective protection against bites of lizard predators.<sup>20</sup> Fibrous ridges in the endocuticle tightly bind the fibres and provide extra structural support.<sup>21</sup> While Wang *et al.*<sup>21</sup> suggested the sclerotisation of the endocuticle in *P. sarcitis kotoensis*, no strong evidence was given to confirm this observation.

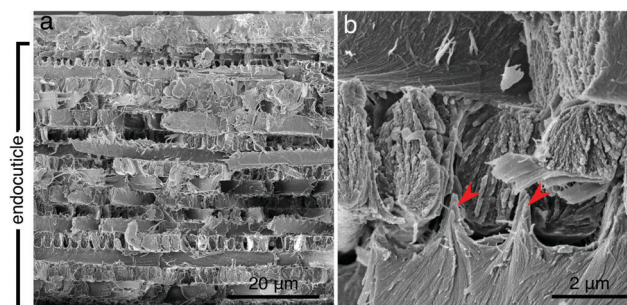


Fig. 1 Microstructure of elytral endocuticle of the weevil, *Pachyrhynchus sarcitis kotoensis*. (a) Multiple sublayers in endocuticle with fibres that arranged in different orientations. (b) Fibrous matrix (red arrows) fills the space between fibres.

<sup>a</sup> Functional Morphology and Biomechanics, Institute of Zoology, Kiel University, Kiel, Germany. E-mail: hrajabi@zoologie.uni-kiel.de, hrajabi@hotmail.com

<sup>b</sup> School of Biosciences, The University of Melbourne, Melbourne, Australia

<sup>c</sup> Department of Life Science, National Taiwan Normal University, Taipei, Taiwan

<sup>d</sup> Department of Mechanical Engineering, University of Guilan, Rasht, Iran

In this study, we first examined the degree of sclerotisation in the endocuticle of the weevil *P. sarcitis kotoensis*. To quantify the effect of the sclerotization on the material properties of the endocuticle, we also measured the stiffness of this layer using nanoindentations. Finally, we used the obtained data in a set of numerical models to test how a sclerotised endocuticle helps the mechanical stability of the insect exoskeleton. Here we present results which have not been reported elsewhere and are of particular importance for understanding the material–function relationships in cuticle as well as the evolution of defence in insects.

### 1.1. Terminology

As in many previous studies,<sup>16,22–25</sup> here we categorised the different cuticular layers based on their specific microstructure. The exocuticle was defined as a layer with thin and dense sublayers. The endocuticle, on the other hand, was defined as a layer with sublayers which are thicker and less dense, compared with those in the exocuticle.<sup>24</sup> The border between the two layers was defined as where the overall arrangement of fibres changes.

## 2. Materials and methods

### 2.1. Ethical statement

The use of the protected *P. sarcitis kotoensis* in the present study was permitted by the Forestry Bureau, Council of Agriculture, Taiwan (no. 1060241435). All the experiments comply with the ethical guidelines at Kiel University, and were performed following the Ordinance on Safety and Health Protection at Workplaces Involving Biological Agents (BioStoffV) launched by the Federal Ministry of Labor and Social Affairs, Germany.

### 2.2. Study animals

Adult *P. sarcitis kotoensis* were collected from Orchid Island, Taiwan, in March and November of 2017. They were fed with the leaves of the known host plant *Leea guineensis* (Leeaceae). The individuals used for nanoindentation, confocal laser scanning microscopy (CLSM), and micro-computed tomography (micro-CT) were deep-frozen at  $-24\text{ }^{\circ}\text{C}$  before sample preparation. The individual used for staining, was anesthetized by carbon dioxide and directly used in the microscopy procedure.

### 2.3. Confocal laser scanning microscopy (CLSM)

Pieces of the frozen elytral cuticle ( $0.5 \times 2.0\text{ mm}^2$ ) of the weevils ( $n = 5$ ) were removed from the body with a sharp razor blade (0.23 mm thick, single-edge blade, Personna, Verona, Virginia, USA). After thawing at room temperature, they were washed with 75% ethanol, embedded in glycerol, placed on glass slides, and covered with cover slips. A confocal laser scanning microscope (Zeiss LSM 700, Carl Zeiss Microscopy, Jena, Germany) equipped with a  $10\times$  objective lens (Zeiss Plan-Apochromat) and four stable solid-state lasers (wavelengths: 405, 488, 555, and 639 nm) was used to scan the samples. The autofluorescence of the samples was detected using four corresponding

emission filters (BP420 – 480, LP490, LP560, and LP640 nm). The colouration of the obtained image was used as a measure of the material composition of the samples as follows: red colour as highly sclerotised cuticle, green colour as less sclerotised and more chitinous cuticle, and blue colour as resilin dominated cuticle. For the details of this method and theory, see Michels and Gorb, 2012.<sup>26</sup>

### 2.4. Scanning electronic microscopy (SEM)

Pieces of the elytral cuticle were removed from the weevils ( $n = 5$ ) and air dried at room temperature. After dehydration, they were broken into several smaller pieces and glued on SEM stubs with carbon-bearing double-sided adhesive Leit-tabs (Plano GmbH, Wetzlar, Germany) and Leit-C conductive carbon cement (Neubauer, Muenster, Germany). The specimens were sputter-coated with  $\sim 9\text{ nm}$ -thick gold–palladium in a sputter coater (Leica EM SCD500; Leica Microsystems GmbH, Wetzlar, Germany) and observed in a SEM (Hitachi S4800; Hitachi High-Tech., Tokyo, Japan).

### 2.5. Embedding, microtomy and staining

Elytral pieces ( $1 \times 2\text{ mm}^2$ ) were removed from a freshly sacrificed weevil ( $n = 1$ ), fixed in a solution of 2.5% glutardialdehyde at  $4\text{ }^{\circ}\text{C}$  for 48 h, washed with phosphate-buffered saline (PBS) for 20 min at  $4\text{ }^{\circ}\text{C}$  twice, and then fixed in 1% OsO<sub>4</sub> solution for 1 h at  $4\text{ }^{\circ}\text{C}$ . After the fixation, the specimens were washed with double distilled water for 20 min at  $4\text{ }^{\circ}\text{C}$  twice, followed by washing in a series of ethanol at  $4\text{ }^{\circ}\text{C}$  for dehydration (30% ethanol for 15 min, 50% ethanol for 15 min, 70% ethanol for 20 min, 95% ethanol for 10 min, 95% ethanol for 20 min, 100% ethanol for 20 min, 100% ethanol on molecular sieve twice). A mixture of 100% ethanol and Epon 812 (Glycidether 100; Carl Roth GmbH, Karlsruhe, Germany) was used in the following proportions for infiltration of Epon: 1 : 1 for 30 min twice, and 1 : 2 for 90 min twice. Elytral samples were then placed in Epon for 24 h and transferred to another container with Epon for 6 h twice. After the infiltration, the samples with Epon were placed in an oven at  $60\text{ }^{\circ}\text{C}$  for 48 h for polymerization. The polymerized embedded samples were cut into semi-thin sections (thickness:  $0.2\text{--}1\text{ }\mu\text{m}$ ) using a Leica EM UC7 ultramicrotome (Leica Microsystems GmbH, Wetzlar, Germany). The sections were stained with Heidenhain's Azan, Cason's, and toluidine blue staining for visualization of different components of cuticle.

For Heidenhain's Azan staining, the sections were first soaked in a preheated solution ( $56\text{ }^{\circ}\text{C}$ ) of 100 ml distilled water, 0.1 g azocarmine G, and 1 ml 100% acetic acid for 20 min. After the first mixture, they were rinsed with distilled water and soaked in the second solution of 0.1 ml aniline and 100 ml 90% ethanol for 15 min. Next, the sections were transferred to the third solution of 100 ml 96% ethanol and 1 ml acetic acid for 1 min. Then, they were incubated in 5% phosphotungstic acid for 150 min and rinsed with distilled water. Finally, the sections were bathed in the fourth solution of 0.5 g aniline blue, 2 g orange G, 100 ml distilled water and 8 ml 100% acetic acid

for 3 h, and rinsed with distilled water (adopted from Romeis *et al.*<sup>27</sup>).

For Cason's staining, the sections were soaked in a solution of 200 ml distilled water, 1 g phosphotungstic acid crystals, 2 g orange G, 1 g aniline blue, and 3 g acid fuchsin for 5 min at 60 °C, and then rinsed with 5% acetic acid followed by 100% ethanol.<sup>28</sup>

For toluidine blue staining, the sections were soaked in toluidine blue solution of 100 ml distilled water, 0.5 g toluidine blue and 1 g sodium borate for 30–60 s. They were then briefly rinsed with running tap water.

All the images of the stained sections were taken using a Zeiss Axioplan light microscope (Zeiss, Oberkochen, Germany) equipped with a 20× lens, and overlaid, stitched and processed in Photoshop (CS5) software.

## 2.6. Nanoindentation

Small pieces of the frozen elytral cuticle ( $2 \times 2 \text{ mm}^2$ ) were cut from the body with a sharp razor blade. The elytral pieces were glued on cylindrical sample holders (diameter: 12.74 mm; height: 12.55 mm) with the cyanoacrylate adhesive (ERGO 5925, Kistling, Zurich, Switzerland). Then they were completely thawed at room temperature. In order to obtain a flat surface on the samples for indentation, we polished them by sandpapers with grain diameters of 3 μm, 1 μm and 0.3 μm (693102, 693103, 693104; Buehler, Lake Bluff, IL, USA). To measure the elastic modulus of the endocuticle in the normal direction, we removed the epi- and exocuticle layers by polishing them off. To maintain the hydration of the samples during indentation, we surrounded them with wet cotton and covered the cotton with parafilm (Bemis Company, Inc., Neenah, Wisconsin, USA).

The samples were tested within less than 1 h after preparation to ensure their hydration. Indentations were performed using a nanoindenter (Nano Indenter SA2, MTS Nano Instruments, Oak Ridge, TN, USA) equipped with a standard Berkovich indenter tip. The samples were loaded under a constant velocity of  $30 \text{ nm s}^{-1}$ . For the analysis of the obtained results, we averaged the data points from 0.1 μm of the stable region of the elastic modulus-penetration depth curve (always chosen from the data points between 1.1 μm and 1.3 μm). For each individual, we measured 2 to 3 elytral pieces by performing ~10 indentations on each piece and averaged the data to represent the elastic modulus of the elytra of that individual. In all, 5 individuals were used for the measurements in the normal direction ( $n = 5$ ) and 6 individuals were used for the measurements in the transverse direction ( $n = 6$ ).

## 2.7. Micro-computed tomography

Micro-CT was used to characterize the three-dimensional (3D) geometry of the exoskeleton of *P. sarcitis kotoensis*. An air-dried individual was fixed on a sample holder with wax and scanned by a Skyscan 1172 micro-CT scanner (Bruker microCT, Kontich, Belgium) with a resolution of ~1 μm at a source voltage of 40 kV and a current of 250 μA. The scanned images were reconstructed in the NRecon package (SkyScan, Kontich, Belgium) and were used for numerical analysis (see Data/Code availability).

## 2.8. Numerical analysis

### 2.8.1. Effect of sclerotisation on the mechanical behaviour of cuticle.

Numerical analyses were carried out to determine the extent to which the sclerotisation affects the mechanical behaviour of the exoskeleton of the weevil *P. sarcitis kotoensis*. For this purpose, a geometric model of a section of the insect abdomen was developed based on the micro-CT data. This was done using the finite element (FE) software package ABAQUS v.6.14 (Simulia, Providence, RI, USA). The insect abdomen forms a hemisphere with an internal radius of 2.81 mm and a thickness of 177.61 μm. Based on the microscopy observations, we partitioned the model into 3 layers across the thickness: a 1 μm-thick layer of epicuticle, a 3.87 μm-thick layer of exocuticle, and a 172.74 μm-thick layer of endocuticle, from outside to inside.<sup>21</sup> The developed models were then meshed with four-node bilinear axisymmetric quadrilateral elements with reduced integration (CAX4R).<sup>29</sup>

Two gradients of the elastic modulus were assigned to the geometric model (Fig. 2a and b). This was performed by introducing a temperature field and then defining the elastic modulus as a function of temperature, similar to that explained by Eshghi *et al.*<sup>30</sup> The first model, referred to as the 'reference model', had the same elastic modulus as the elytral cuticle of *P. sarcitis kotoensis*, measured by nanoindentations (Fig. 2a). The second model, called the 'typical model', had an exponential gradient of the elastic modulus within each layer, similar to that observed in a typical cuticle<sup>31</sup> (Fig. 2b). The strength and Poisson's ratio of the cuticle were set to be 250 MPa<sup>32</sup> and 0.3,<sup>31</sup> respectively. The failure was defined when von Mises stress in an element of the model exceeded the strength of the cuticle.

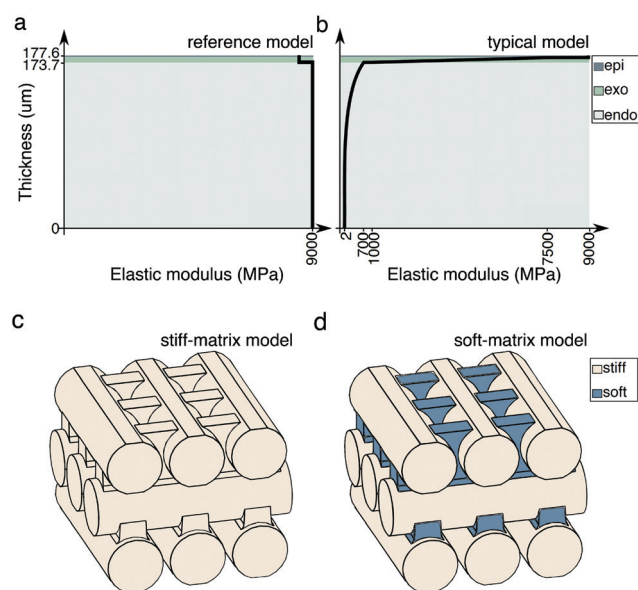


Fig. 2 Modelling of elytral cuticle of the weevil, *Pachyrhynchus sarcitis kotoensis*. (a and b) Gradients of the elastic modulus across the thickness of whole cuticle models: 'reference model' (a), 'typical model' (b). Thick black lines represent changes of the elastic modulus across the thickness of the models. (c and d) Endocuticle models: 'stiff-matrix model' (c) with a sclerotised matrix, and 'soft-matrix model' (d) with a resilin-rich matrix.

The implicit solver ABAQUS/Standard was used for the computational analysis. The models were subjected to a uniform compression using a rigid plate. A surface to surface contact pair with 'hard contact' behaviour in the normal direction was defined to avoid the penetration of the rigid plate into the models.<sup>29</sup> The displacements at the bottom of the hemispherical models were fixed in all directions. Prior to each simulation, a mesh convergence analysis was performed to obtain data which were not dependent on mesh size.

**2.8.2. Effect of the sclerotised matrix on the mechanical behaviour of the endocuticle.** We developed two other FE models to determine the effect of the sclerotised matrix between the fibres on the stiffness of the insect endocuticle (Fig. 2c and d). The models were designed to represent a small periodic volume of the endocuticle. Both models consisted of three layers, and each layer had three cylindrical fibres. The fibres were identical in shape with a length of 14  $\mu\text{m}$  and a diameter of 4  $\mu\text{m}$ .<sup>21</sup> For ease of modelling, the fibres in the successive layers were rotated for 90° with respect to each other. The space between the fibres was filled by a matrix emerged from fibres in a layer below. The models were meshed using the general purpose four-node tetrahedral elements (C3D4) with second-order accuracy.

In both models, fibres were assumed to be sclerotised with an elastic modulus of 9 GPa, a Poisson's ratio of 0.3, a strength of 250 MPa and a density of 1200  $\text{kg m}^{-3}$ .<sup>31</sup> However, the material properties of the matrix material were set to be different in the two models. The first model, called the 'stiff-matrix model', had a matrix with an elastic modulus equal to that of the sclerotised cuticle. In the second model, called the 'soft-matrix model', the elastic modulus, Poisson's ratio, strength and density were set to be 2 MPa, 0.49, 4 MPa, and 1000  $\text{kg m}^{-3}$ , respectively.<sup>31</sup> These values correspond to the properties of the soft, resilin-bearing matrix in a typical insect cuticle.<sup>5,33</sup>

The bottoms of the models were fixed in all directions. A rigid plate was used to apply a 4 mN compressive force, in the form of a uniform pressure, to the upper surface of the models. The analysis was conducted using a dynamic explicit technique.<sup>29</sup> To avoid the penetration of the rigid plate into the models, a surface to surface contact pair by consideration of a 'hard contact' in the normal direction was employed.<sup>29</sup> The use of friction in the tangential direction helped to restrain the sliding of the fibres.<sup>29</sup> Prior to each simulation, a mesh convergence analysis was conducted to eliminate the effect of element size on the results.

## 2.9. Statistical analysis

No statistical methods were used to predetermine sample size. All the statistical tests in the present study are two-tailed and performed in R 3.4.4.<sup>34</sup> Assumptions of normality and homogeneity of variances were tested by Shapiro–Wilk test and Bartlett's test before further analysis. We compared the elastic moduli of the exocuticle of the weevil from the previous study<sup>21</sup> with that of the endocuticle measured in the normal direction and in the transvers direction by analysis of variance (ANOVA)

followed with *post hoc* Tukey honest significant differences (Tukey HSD) for multiple comparison.

## 3. Results

### 3.1. High degree of sclerotisation in the endocuticle

Red, green and blue colours in the CLSM image shown in Fig. 3a indicate highly sclerotised, less sclerotised and resilin-rich cuticle, respectively. As seen here, the exocuticle was dominated by red autofluorescence, and the endocuticle was on the other hand dominated by orange and yellow colours (*i.e.* a mixture of more red and green and less blue). The results, therefore, suggested that the elytral cuticle of *P. sarcitis kotoensis* was generally very sclerotised. Though the red colour at the outer parts of the cuticle indicated a higher degree of sclerotisation than the inner parts, the inner parts showed very little blue colour, suggesting the presence of only a small amount of resilin-rich areas in the endocuticle.

The staining results confirmed the observation of the sclerotised endocuticle in the CLSM image. Highly sclerotised regions are either refractive to staining or were stained in brown, orange and yellow in Fig. 3b and c. Other sclerotised regions in Fig. 3c were stained in pink. Soft, proteinous cuticle was stained in blue in Fig. 3b and c, and was restricted to the cross section of the fibres. Similar results were obtained with toluidine blue staining (Fig. 3d). Here dark blue colour showed the soft part of the cuticle, which was restricted to the fibres (see inset in Fig. 3d). However, the surrounding matrix, which filled the space between fibres, was sclerotised (red arrows in the inset of Fig. 3d).

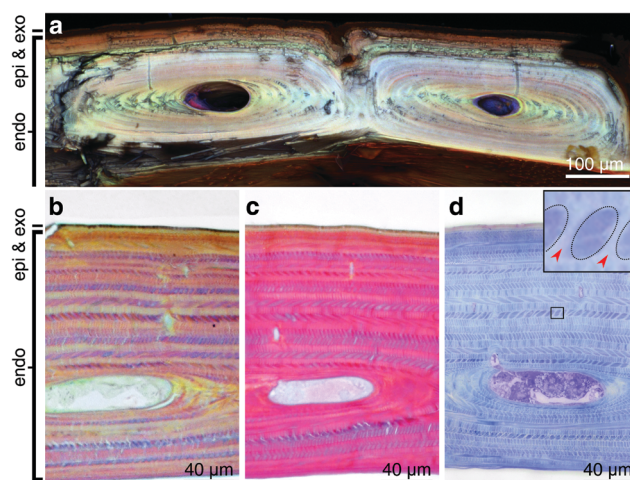


**Fig. 3** Sclerotisation of elytral cuticle of the weevil, *Pachyrhynchus sarcitis kotoensis*. (a) Confocal laser scanning microscopy (CLSM) image of the cross section of the elytra. Degrees of sclerotisation (more to less): red, orange, yellow and green. (b–d) Results of (b) Heidenhain's Azan, (c) Cason's, and (d) toluidine blue staining methods. In (b) and (c), highly sclerotised regions (more to less): brown, orange and yellow; in (c), less sclerotised regions: pink. In (d), dark blue indicates soft cuticle. The inset shows three fibres (circled by black dotted lines) surrounded by a stiff matrix (pointed by red arrows).

### 3.2. Stiffness of the endocuticle in different directions

We measured the elastic modulus of the endocuticle in the normal (*i.e.* on the dorsal surface) and the transverse directions (*i.e.* on the cross-section). The elastic moduli of the endocuticle in the normal and transverse directions were  $8.97 \pm 0.31$  GPa (mean  $\pm$  s.d.) and  $10.17 \pm 0.95$  GPa, respectively. We compared these values with the elastic modulus of the exocuticle in the normal direction ( $8.40 \pm 0.87$  GPa,  $n = 5$ ; data extracted from Wang *et al.*<sup>21</sup>) (Fig. 4; ANOVA,  $F_{2,15} = 7.465$ ,  $P = 0.007$ ). When indented in the normal direction, the endocuticle was even slightly stiffer than the exocuticle by  $\sim 7\%$  (Tukey HSD,  $P = 0.503$ ) (Fig. 4). When indented in the transverse direction, the endocuticle was significantly stiffer than the exocuticle by  $\sim 21\%$  (Tukey HSD,  $P = 0.006$ ; Fig. 4). No significant difference was found between the elastic moduli of the endocuticle in the normal and transverse directions (Tukey HSD,  $P = 0.059$ ).

### 3.3. Effect of sclerotisation on the mechanical resistance of the cuticle

To test the effect of the sclerotised endocuticle, we developed two models: 'reference model' and 'typical model' (Fig. 2a and b) based on the data from micro-CT scanning of the weevil exoskeleton. The former one had the same elastic modulus as the elytral cuticle of the weevil. The latter had a soft endocuticle with an exponential gradient of the elastic modulus across the cuticle thickness, similar to what is observed in a typical insect cuticle.<sup>31</sup> When subjected to compression, the 'reference model' withstood  $\sim 6$  times the force required to fail the 'typical model' (Fig. 5a). To resist the same load, the 'typical model' should increase the thickness by  $\sim 9$  times (Fig. 5b).

Next, we tested the effect of the sclerotised matrix in the endocuticle of the weevil on its mechanical resistance by

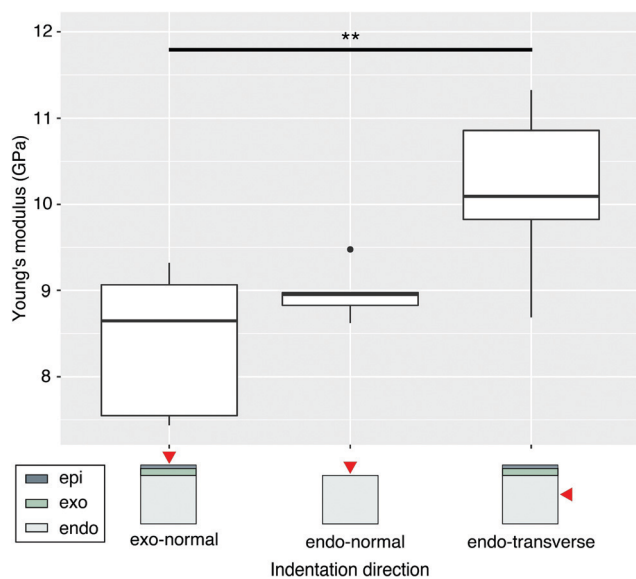


Fig. 4 Elastic moduli of elytral cuticle of the weevil *Pachyrhynchus sarcitis kotoensis*. Results of nanoindentation. exo-: exocuticle, endo-: endocuticle. Solid dot in the box-and-whisker plot: outlier; \*\* $P < 0.01$ . exo-normal,  $n = 5$ , endo-normal,  $n = 5$ , endo-transverse,  $n = 6$ .

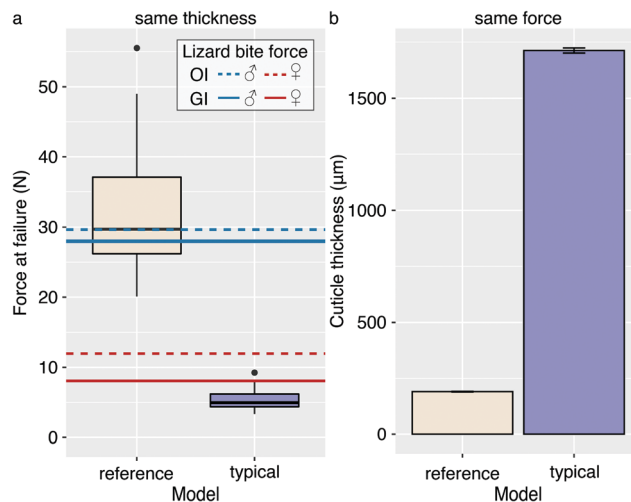


Fig. 5 Effect of endocuticle sclerotisation. (a) The force required to fail the insect exoskeleton when the 'reference model' and 'typical model' both have the same thickness. The horizontal lines show the maximal bite force of the lizard predator, *Japalura swinhonis*, from two different populations, from ref. 20: GI, Green Island; OI, Orchid Island. In box-and-whisker plots: centre line, median; box limits, upper and lower quartiles; whiskers,  $1.5 \times$  interquartile range; points, outliers. (b) The cuticle thickness of the 'typical model' and 'reference model' when having the same load-carrying capacity. Error bar: standard error.

developing two additional FE models: 'stiff-matrix model' and 'soft-matrix model'. The two models differed only in the elastic modulus of the matrix material, and not the fibres (Fig. 2c and d). The elastic modulus of the matrix in the 'stiff-matrix model' equals that of the sclerotised cuticle of the studied weevil. The 'soft-matrix model', in contrast, had a soft matrix similar to that of a typical cuticle.<sup>22,25</sup> When under an external pressure, the sclerotised matrix increased the stiffness of the whole model by  $\sim 10$  times.

## 4. Discussion

Our study showed sclerotisation in all cuticular layers of *P. sarcitis kotoensis* and highlighted the first record of sclerotized endocuticle in insects. Our results also suggested a pronounced increase in the mechanical stability of the cuticle by possessing sclerotised endocuticle. The endocuticle of most insects is soft and resilin-rich,<sup>11–13,35,36</sup> while in that of *P. sarcitis kotoensis*, the matrix surrounding the fibres is especially sclerotised. The unique material property of the weevil's endocuticle provides a novel example in the study of insect cuticles.

Predation pressure drives the evolution of defence in animals. Varieties of defence strategies have evolved to increase the survival of many preys.<sup>37</sup> An effective defensive strategy in insects is to form a mechanically robust exoskeleton, which can be achieved by an increased body wall thickness, thick fibres, sclerotisation of the outer layers of the cuticle, *etc.*<sup>21,38–40</sup> In *P. sarcitis kotoensis*, interestingly, not only the outer layers of the cuticle, but also the typically soft endocuticle has become sclerotised. The stiffness of the endocuticle is independent from the direction of the measurement, indicating that it is a stiff composite in general. The sclerotized exo- and endocuticle,

together, have enabled the weevil to achieve an extraordinarily stiff exoskeleton, having a high load-carrying capacity for defending against predatory bites.

According to our numerical simulations, the force required to fail the cuticle of the weevil is just above the mechanically measured bite force of the lizard predators (Fig. 5a; yellow box) (bite force of the lizard predator, *Japalura swinhonis*: Orchid island male:  $29.66 \pm 9.62$  N, Orchid island female:  $12.03 \pm 2.80$  N, Green island male:  $27.97 \pm 9.55$  N, Green island female:  $8.14 \pm 2.42$  N<sup>20</sup>). This indicates that without a stiff endocuticle, *P. sarcitis kotoensis* can be consumed by the lizard predators, since the maximal bite force of the female lizards exceeds the force required to break the 'typical model' (Fig. 5a; purple box). If the 'typical model' cuticle has to withstand the same external load, it must increase the cuticle thickness by  $\sim 9$  times (Fig. 5b). This would lead to more energy expenditure to form a thick cuticle and could cause an obstacle in locomotion.

Though the sclerotised cuticle enhances the load-carrying capacity of the insect exoskeleton, it comes with a considerable biomechanical disadvantage. The weevils have to sacrifice the toughness of their exoskeleton, *i.e.* the resistance to fracture. This is evident in the fracture behaviour of the exoskeleton of the mature *P. sarcitis kotoensis*, reported in our previous study.<sup>21</sup> In comparison with the highly sclerotised cuticle of mature weevils, teneral weevils (referring to the individuals within 5 days of the emergence from the pupal chambers in ref. 21) exhibited only minor cuticle sclerotisation. The exoskeleton of mature weevils could withstand a force  $\sim 150$  times higher than that of teneral weevils before failure.<sup>21</sup> However, when the ultimate strength was reached, the exoskeleton of mature weevils fractured catastrophically. In contrast, the exoskeleton of teneral weevils had a slow, mostly recoverable failure.<sup>21</sup>

Such an exceptionally sclerotised endocuticle, although it decreases the toughness of the exoskeleton, increases the strength of the exoskeleton and secures the weevils with a robust body armour. This novel strategy, utilized by *P. sarcitis kotoensis*, sheds new lights on our understanding of the relationship between the material properties and functions of insect cuticle. Further studies estimating the energy expenditure required to synthesize sclerotised cuticle can help us to better understand the trade-offs in the evolution of body armour in insects.

## Author contributions

SNG and HR conceptualized the study. L-YW, SNG, and HR designed the study. L-YW, MJ, EA, and HR collected the data. L-YW and HR analysed the data. L-YW, MJ, SNG, and HR discussed the results. L-YW drafted the manuscript. HR revised the manuscript. MJ, EA, C-PL, and SNG reviewed and edited the manuscript. HR, C-PL, and SNG supervised the study. C-PL and SNG acquired the research funding. L-YW, and HR contributed to revision. All authors gave final approval for publication.

## Data/code availability

All nanoindentation data, reconstructed micro-CT data, R code, and finite element models collected/used in this study are available on Figshare: DOI: 10.6084/m9.figshare.7398641.

## Conflicts of interest

The authors declare no competing interests.

## Acknowledgements

This study was supported by DAAD Short-term Research Grants (57378443) to L-YW and a research grant of the Ministry of Science and Technology of Taiwan (MOST 106-2311-B-003-004-MY3, 107-2311-B-003-002-MY3) to C-PL.

## References

- 1 D. Grimaldi, M. S. Engel and M. S. Engel, *Evolution of the Insects*, Cambridge University Press, 2005.
- 2 P. J. Gullan and P. S. Cranston, *The insects: an outline of entomology*, John Wiley & Sons, 2014.
- 3 R. M. May, How many species are there on earth?, *Science*, 1988, **241**(4872), 1441–1449.
- 4 T. L. Hopkins and K. J. Kramer, Insect cuticle sclerotization, *Annu. Rev. Entomol.*, 1992, **37**(1), 273–302.
- 5 J. F. Vincent and U. G. Wegst, Design and mechanical properties of insect cuticle, *Arthropod Struct. Dev.*, 2004, **33**(3), 187–199.
- 6 A. C. Neville, *Biology of the arthropod cuticle*, Springer Science & Business Media, 2012.
- 7 A. C. Neville, *Biology of the arthropod cuticle*, Springer-Verlag, 1975.
- 8 T. Weis-Fogh, A rubber-like protein in insect cuticle, *J. Exp. Biol.*, 1960, **37**(4), 889–907.
- 9 H. R. Hepburn and I. Joffe, On the material properties of insect exoskeletons, in *The insect integument*, ed. H. R. Hepburn, Elsevier, Amsterdam, 1976, pp. 207–235.
- 10 S. Gunderson and R. Schiavone, The insect exoskeleton: a natural structural composite, *JOM*, 1989, **41**(11), 60–63.
- 11 E. Appel, L. Heepe, C. P. Lin and S. N. Gorb, Ultrastructure of dragonfly wing veins: composite structure of fibrous material supplemented by resilin, *J. Anat.*, 2015, **227**(4), 561–582.
- 12 H. Rajabi, A. Shafiei, A. Darvizeh, S. Gorb, V. Dürr and J.-H. Dirks, Both stiff and compliant: morphological and biomechanical adaptations of stick insect antennae for tactile exploration, *J. R. Soc., Interface*, 2018, **15**(144), 20180246.
- 13 M. Schmitt, T. H. Büscher, S. N. Gorb and H. Rajabi, How does a slender tibia resist buckling? Effect of material, structural and geometric characteristics on buckling behaviour of the hindleg tibia in stick insect postembryonic development, *J. Exp. Biol.*, 2018, **221**(4), jeb173047.
- 14 H. R. Hepburn and A. Ball, On the structure and mechanical properties of beetle shells, *J. Mater. Sci.*, 1973, **8**(5), 618–623.

- 15 A. Neville and B. Luke, A two-system model for chitin-protein complexes in insect cuticles, *Tissue Cell*, 1969, **1**(4), 689–707.
- 16 T. van de Kamp, A. Riedel and H. Greven, Micromorphology of the elytral cuticle of beetles, with an emphasis on weevils (Coleoptera: Curculionidae), *Arthropod Struct. Dev.*, 2016, **45**(1), 14–22.
- 17 Y. Bouligand, Twisted fibrous arrangements in biological materials and cholesteric mesophases, *Tissue Cell*, 1972, **4**(2), 189–217.
- 18 H. R. Hepburn, Some mechanical properties of crossed fibrillar chitin, *J. Insect Physiol.*, 1972, **18**(5), 815–825.
- 19 H. R. Hepburn and D. C. Roberts, Stiffness and tanning of sclerites, *J. Insect Physiol.*, 1975, **21**(11), 1741–1746.
- 20 L.-Y. Wang, W.-S. Huang, H.-C. Tang, L.-C. Huang and C.-P. Lin, Too hard to swallow: a secret secondary defence of an aposematic insect, *J. Exp. Biol.*, 2018, **221**(2), jeb172486.
- 21 L.-Y. Wang, H. Rajabi, N. Ghoroubi, C.-P. Lin and S. N. Gorb, Biomechanical strategies underlying the robust body armour of an aposematic weevil, *Front. Physiol.*, 2018, **9**, 1410.
- 22 N. Barbakadze, S. Enders, S. Gorb and E. Arzt, Local mechanical properties of the head articulation cuticle in the beetle *Pachnoda marginata* (Coleoptera, Scarabaeidae), *J. Exp. Biol.*, 2006, **209**(4), 722–730.
- 23 M. A. Meyers, P. Y. Chen, A. Y. M. Lin and Y. Seki, Biological materials: Structure and mechanical properties, *Prog. Mater. Sci.*, 2008, **53**(1), 1–206.
- 24 T. van de Kamp and H. Greven, On the architecture of beetle elytra, *Entomol. Heute*, 2010, **22**, 191–204.
- 25 S. S. Singh, M. A. Jansen, N. M. Franz and N. Chawla, Microstructure and nanoindentation of the rostrum of *Curculio longinasus* Chittenden, 1927 (Coleoptera: Curculionidae), *Mater. Charact.*, 2016, **118**, 206–211.
- 26 J. Michels and S. N. Gorb, Detailed three-dimensional visualization of resilin in the exoskeleton of arthropods using confocal laser scanning microscopy, *J. Microsc.*, 2012, **245**(1), 1–16.
- 27 B. Romeis, in *Mikroskopische Technik*, ed. M. Mulisch, U. Welsch, Spektrum Akademischer, Heidelberg, 2010, pp. 209, 217–218.
- 28 J. E. Cason, A rapid one-step Mallory-Heidenhain stain for connective tissue, *Stain Technol.*, 1950, **25**(4), 225–226.
- 29 *ABAQUS v6.14, Abaqus Analysis User's Guide*, Dassault Systèmes Simulia Corp., Providence, RI, USA, 2014.
- 30 S. H. Eshghi, M. Jafarpour, A. Darvizeh, S. Gorb and H. Rajabi, A simple, high-resolution, non-destructive method for determining the spatial gradient of the elastic modulus of insect cuticle, *J. R. Soc., Interface*, 2018, **15**(145), 20180312.
- 31 H. Rajabi, M. Jafarpour, A. Darvizeh, J.-H. Dirks and S. N. Gorb, Stiffness distribution in insect cuticle: a continuous or a discontinuous profile?, *J. R. Soc., Interface*, 2017, **14**(132), 20170310.
- 32 E. Parle, J.-H. Dirks and D. Taylor, Damage, repair and regeneration in insect cuticle: The story so far, and possibilities for the future, *Arthropod Struct. Dev.*, 2017, **46**(1), 49–55.
- 33 D. Klocke and H. Schmitz, Water as a major modulator of the mechanical properties of insect cuticle, *Acta Biomater.*, 2011, **7**(7), 2935–2942.
- 34 R Core Team, *R: A Language and Environment for Statistical Computing*, R Foundation for Statistical Computing, Vienna, Austria, 2018.
- 35 A. R. Varman, Resilin in the cuticle of physogastric queen termites, *Experientia*, 1980, **36**(5), 564.
- 36 H. Rajabi, A. Shafiei, A. Darvizeh and S. Gorb, Resilin microjoints: a smart design strategy to avoid failure in dragonfly wings, *Sci. Rep.*, 2016, **6**, 39039.
- 37 P. A. Abrams, The evolution of predator-prey interactions: theory and evidence, *Annu. Rev. Ecol. Syst.*, 2000, **31**(1), 79–105.
- 38 S. Andersen, M. G. Peter and P. Roepstorff, Cuticular sclerotization in insects, *Comp. Biochem. Physiol., Part B: Biochem. Mol. Biol.*, 1996, **113**(4), 689–705.
- 39 J. F. Vincent, Arthropod cuticle: a natural composite shell system, *Composites, Part A*, 2002, **33**(10), 1311–1315.
- 40 M. Kohane, A. Daugele, H. Kutomi, L. Charlson, A. Wyrobek and J. Wyrobek, Nanoscale in vivo evaluation of the stiffness of *Drosophila melanogaster* integument during development, *J. Biomed. Mater. Res., Part A*, 2003, **66**(3), 633–642.